

Physical properties and radius variations in the HAT-P-5 planetary system from simultaneous four-colour photometry

John Southworth¹, L. Mancini², P. F. L. Maxted¹, I. Bruni³, J. Tregloan-Reed¹,
M. Barbieri⁴, N. Ruocco^{5,6}, P. J. Wheatley⁷

¹ *Astrophysics Group, Keele University, Newcastle-under-Lyme, ST5 5BG, UK*

² *Max Planck Institute for Astronomy, Königstuhl 17, 69117 – Heidelberg, Germany*

³ *INAF – Osservatorio Astronomico di Bologna, Via Ranzani 1, 40127 Bologna, Italy*

⁴ *Observatoire de la Côte d’Azur, 06304 Nice Cedex 4, France*

⁵ *Astrocampaia, Sez. Stabia Penisola Sorrentina, Italy*

⁶ *Unione Astrofili Italiani, Variable Stars Division, Italy*

⁷ *Department of Physics, University of Warwick, Coventry, CV4 7AL, UK*

25 May 2018

ABSTRACT

The radii of giant planets, as measured from transit observations, may vary with wavelength due to Rayleigh scattering or variations in opacity. Such an effect is predicted to be large enough to detect using ground-based observations at multiple wavelengths. We present defocussed photometry of a transit in the HAT-P-5 system, obtained simultaneously through Strömgren *u*, Gunn *g* and *r*, and Johnson *I* filters. Two more transit events were observed through a Gunn *r* filter. We detect a substantially larger planetary radius in *u*, but the effect is greater than predicted using theoretical model atmospheres of gaseous planets. This phenomenon is most likely to be due to systematic errors present in the *u*-band photometry, stemming from variations in the transparency of Earth’s atmosphere at these short wavelengths. We use our data to calculate an improved orbital ephemeris and to refine the measured physical properties of the system. The planet HAT-P-5 b has a mass of $1.06 \pm 0.11 \pm 0.01 M_{\text{Jup}}$ and a radius of $1.252 \pm 0.042 \pm 0.008 R_{\text{Jup}}$ (statistical and systematic errors respectively), making it slightly larger than expected according to standard models of coreless gas-giant planets. Its equilibrium temperature of 1517 ± 29 K is within 60 K of that of the extensively-studied planet HD 209458 b.

Key words: stars: planetary systems — stars: fundamental parameters — stars: individual: HAT-P-5

1 INTRODUCTION

Of the known extrasolar planets, those which transit their parent stars comprise a rich source of information on the formation and evolution of gas giants. The physical properties of transiting extrasolar planets (TEPs) can be determined – with a little help from stellar evolutionary theory – to precisions approaching a few percent¹ (e.g. Torres et al. 2008; Southworth 2009). The radii of the known TEPs are of particular interest as indicators of the internal structure and heating mechanisms of irradiated giant planets (e.g. Fortney et al. 2007; Batygin et al. 2009). Also, the opacities of different species in the atmospheres of TEPs change with wavelength, causing variations of their radii as measured from transit light curves. These wavelength-dependent variations can be used to probe the atmospheric composition of the objects (see Burrows et al. 2007).

Fortney et al. (2008) divided the known gas-giant TEPs into two classes according to the presence of appreciable atmospheric opacity from oxidised titanium and vanadium. They calculated the observed radius of a planet with a radius of $1.20 R_{\text{Jup}}$ at 1 bar pressure and a surface gravity of 15 m s^{-2} , for wavelengths of 0.3–30 μm . pM-class planets have high TiO and VO opacity leading to temperature inversions and an increased transit-derived radius over a broad range of optical wavelengths. These objects are predicted to have apparent radii which are the smallest at the bluest optical wavelengths (< 370 nm) and the greatest at 450–700 nm, the difference being 4% for the $1.20 R_{\text{Jup}}$ planet and even larger for one with a lower surface gravity (larger atmospheric scale height). By contrast, the pL planets are less highly irradiated and have negligible TiO and VO opacity. Their transit radii are predicted to be smaller and less variable, with narrow peaks around the NaI 589 nm and KI 768 nm doublets. A similar variation for pL planets was found by Burrows et al. (2010) for the case of HD 209458.

¹ See: <http://www.astro.keele.ac.uk/~jkt/tepcat/>

Table 1. Log of the observations presented in this work. N_{obs} is the number of observations and ‘Moon illum.’ is the fractional illumination of the Moon at the midpoint of the transit. The aperture sizes are the radii of the software apertures for the star, inner sky and outer sky, respectively.

Transit	Date	Start time (UT)	End time (UT)	N_{obs}	Exposure time (s)	Filter	Airmass	Moon illum.	Aperture sizes (px)	Scatter (mmag)
1	2010 08 23	20:24	01:33	201	60	Strömgren <i>u</i>	1.00 → 2.01	0.994	17, 30, 50	3.61
1	2010 08 23	20:24	01:33	204	60	Gunn <i>g</i>	1.00 → 2.01	0.994	30, 45, 70	1.20
1	2010 08 23	20:24	01:33	204	60	Gunn <i>r</i>	1.00 → 2.01	0.994	30, 45, 70	0.93
1	2010 08 23	20:24	01:33	199	60	Johnson <i>I</i>	1.00 → 2.01	0.994	27, 45, 65	1.27
2	2011 05 26	21:18	02:47	135	120–100	Gunn <i>r</i>	1.38 → 1.01 → 1.07	0.294	16, 26, 45	0.75
3	2011 07 19	20:39	02:04	176	90–33	Gunn <i>r</i>	1.03 → 1.01 → 1.53	0.861	20, 30, 50	1.53

Zahnle et al. (2009) has shown that sulphur is an important element for opacity in exoplanet atmospheres, and might serve as a probe of the metallicity of TEPs. S_2 opacity becomes large at 240–340 nm for temperatures above 1200 K, and HS absorbs strongly in the wavelength interval 300–460 nm. These effects should lead to large apparent radii at blue-optical and ultraviolet wavelengths. Another relevant phenomenon is Rayleigh scattering, which is proportional to λ^{-4} and so should cause the transit radii of TEPs to be larger at shorter wavelengths. Both effects run opposite to the predictions of Fortney et al. (2008); it is not yet clear which processes dominate the measured radii of exoplanets.

The two well-studied TEPs, in terms of variation of radius over optical wavelengths, are HD 209458 b and HD 189733 b. For the former, Knutson et al. (2007) presented HST grism photometry of two transits divided into ten wavelength intervals covering 290–1030 nm. Differences of radius with wavelength are unclear from these data: Barman (2007) and Sing et al. (2008) found significant variations whereas Knutson et al. (2007) and Southworth (2008) did not. Charbonneau et al. (2002) has found evidence for NaI absorption in the planetary atmosphere based on an earlier dataset (Brown et al. 2001). These characteristics point to a pL classification for HD 209458 b; its moderate equilibrium temperature of $T'_{\text{eq}} = 1459 \pm 12$ K (Southworth 2010) puts it roughly at the boundary between the pL and pM classes. For HD 189733 b, HST observations covering 550–1050 nm (Pont et al. 2008) and 290–570 nm (Sing et al. 2011) returned only gradual radius variations with wavelength, which have been interpreted as indicative of Rayleigh scattering from a high-altitude atmospheric haze. HD 189733 b has $T'_{\text{eq}} = 1191 \pm 20$ K (Southworth 2010) so is firmly in the pL planetary class. There has therefore been no clear detection of TEP radius variations indicative of a pM classification.

HAT-P-5 was discovered by Bakos et al. (2007) and is a comparatively normal TEP system consisting of a $1.2 M_{\odot}$ star orbited by a $1.1 M_{\text{Jup}}$ planet. Its planet is slightly hotter ($T'_{\text{eq}} = 1516 \pm 29$ K) than HD 209458 b so is on the border of the pL and pM classes. Krivov et al. (2011) found a flux excess at 12 and 22 μm indicative of the presence of dust rings at a distance of several AU from the parent star. In this work we present the first follow-up transit photometry of HAT-P-5 obtained since the discovery paper, covering four optical passbands. We probe for radius variations between these passbands and improve the measurements of the physical properties of the system.

2 OBSERVATIONS AND DATA REDUCTION

We observed one full transit of HAT-P-5 on the night of 2010/08/23, using the 2.2 m telescope and BUSCA imager at Calar Alto Astronomical Observatory. BUSCA uses dichroics to split the incoming

Table 2. Excerpts of the light curve of HAT-P-5. The full dataset will be made available at the CDS.

Telescope	Filter	BJD(TDB)	Diff. mag.	Uncertainty
CAHA22	<i>u</i>	2455432.35006	−0.00004	0.00316
CAHA22	<i>u</i>	2455432.56365	−0.00208	0.00582
CAHA22	<i>g</i>	2455432.35006	0.00156	0.00119
CAHA22	<i>g</i>	2455432.56365	0.00004	0.00135
CAHA22	<i>r</i>	2455432.35006	−0.00013	0.00094
CAHA22	<i>r</i>	2455432.56465	0.00144	0.00099
CAHA22	<i>I</i>	2455432.35006	0.00015	0.00129
CAHA22	<i>I</i>	2455432.56465	0.00093	0.00134
Cassini	<i>r</i>	2455708.38967	0.00066	0.00081
Cassini	<i>r</i>	2455708.60776	−0.00120	0.00119
Cassini	<i>r</i>	2455761.36079	−0.00104	0.00115
Cassini	<i>r</i>	2455761.53645	0.01876	0.00195

light into four wavelength intervals, which traverse different arms of the instrument and are incident onto four CCDs. This allows photometry to be obtained in four passbands simultaneously. The arms of the instrument cannot be operated individually: their focus and CCD settings are controlled together. The full field of view is 12×12 arcminutes, which the CCDs sample with a plate scale of $0.176''$ per pixel.

For our observations we chose to have the dedicated BUSCA 109-mm diameter Strömgren *u* and Johnson *I* filters, in the bluest and reddest arms respectively. For the intermediate arms we opted for 50-mm diameter Gunn *g* and *r* filters from the standard Calar Alto filter catalogue. The latter two filters have a better throughput but lead to a reduced field of view: a circle approximately 6 arcmin in diameter. The *g* and *r* filters are also thinner than the *u* and *I* filters, leading to a difference in focus between the two filter sets. We defocussed BUSCA in such a way as to have the *g* and *r* observations more defocussed than those in *u* and *I*, in order to compensate for the lower throughput of the latter two filters.

The amount of defocussing was set by the requirement that the brightest pixel within the point spread function (PSF) of the target and comparison stars (on all four CCDs) have not more than 35 000 counts in one observation. An initial exposure time of 90 s was chosen, which is slightly smaller than our usual value of 120 s (see Southworth et al. 2009a,b) to limit the impact of the bright moon. The CCDs were binned 2×2 in order to shorten the readout time. The autoguider was not defocussed along with BUSCA, so could be used to maintain the pointing of the telescope.

We observed two transits of HAT-P-5 in May and July 2011,

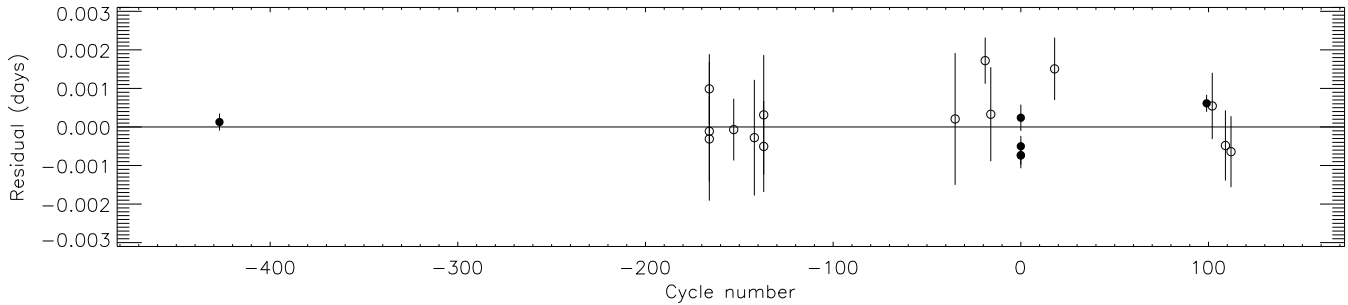


Figure 1. Plot of the residuals of the timings of mid-transit of HAT-P-5 versus a linear ephemeris. The timings obtained by amateur astronomers are plotted using open circles.

using BFOSC mounted on the 1.52 m G. D. Cassini Telescope² at Loiano Observatory, Italy. For more information on the use of this instrument for defocussed photometry see Southworth et al. (2010, 2011). Both transits were observed through a Gunn r filter. The second transit was curtailed by cloud before egress. It also suffered from the gradual drift of the telescope back into focus over the night, requiring the exposure time to be successively reduced from the original 90 s down to 33 s. As with BUSCA, the telescope pointing was maintained using the autoguider. A summary of the observational data is given in Table 1.

One further transit was observed by NR using a 25 cm aperture Meade LX200 telescope sited near Sorrento, Italy (latitude $40^{\circ} 37' 07.37''$ North, longitude $14^{\circ} 21' 27.46''$ East, altitude 275 m above sea level). The CCD used was an SBIG ST7 operating at a plate scale of $1.16'' \text{ px}^{-1}$, mounted behind an r filter. Data reduction was performed using MaxIm DL Pro 5³ following standard procedures.

Several images were taken with the telescopes properly focussed, to verify that there were no faint stars within the defocussed PSF of HAT-P-5. We find no evidence of a second star near the PSF of our star of interest, and conclude that the transit is not diluted by contaminating light. This agrees with Daemgen et al. (2009), who obtained high-resolution observations of HAT-P-5 as part of a high-speed ‘lucky’ imaging survey of twelve TEP host stars.

Data reduction was undertaken using standard methods. Aperture photometry was performed using the IDL⁴/ASTROLIB⁵ implementation of DAOPHOT (Stetson 1987). The apertures were placed by hand and shifted to account for pointing variations, which were measured by cross-correlating each image against a reference image. We tried a wide range of aperture sizes and retained those which gave photometry with the lowest scatter compared to a fitted model (see below). We find that the shape of the light curve is very insensitive to the choice of aperture sizes, and to whether flat fields are used in the reduction process. The times of observation were converted from UTC to barycentric Julian date on the TDB timescale, using the IDL procedures of Eastman et al. (2010).

Differential photometry was obtained using an optimal ensemble of comparison stars (Southworth et al. 2009a) combined with a polynomial fit to the data outside transit. The choice of comparison

Table 3. Times of minimum light of HAT-P-5 and their residuals versus the ephemeris derived in this work.

Time of minimum BJD(TDB) – 2400000	Cycle no.	Residual (JD)	Reference
54241.77700 ± 0.00022	-427.0	0.00013	Bakos et al. (2007)
54969.56817 ± 0.00110	-166.0	-0.00031	Gregorio (AXA)
54969.56837 ± 0.00180	-166.0	-0.00011	Mendez (AXA)
54969.56947 ± 0.00090	-166.0	0.00099	Naves (AXA)
55005.81857 ± 0.00080	-153.0	-0.00007	Norby (AXA)
55036.49157 ± 0.00150	-142.0	-0.00028	Srdoc (AXA)
55050.43371 ± 0.00118	-137.0	-0.00051	Brát (TRESKA)
55050.43453 ± 0.00155	-137.0	0.00031	Trnka (TRESKA)
55334.85873 ± 0.00171	-35.0	0.00021	Shadick (TRESKA)
55379.47582 ± 0.00060	-19.0	0.00172	Vila’agi (TRESKA)
55387.83985 ± 0.00122	-16.0	0.00033	Garlitz (TRESKA)
55432.45534 ± 0.00066	0.0	0.00024	This work (u)
55432.45436 ± 0.00033	0.0	-0.00074	This work (g)
55432.45460 ± 0.00027	0.0	-0.00050	This work (r)
55432.45437 ± 0.00025	0.0	-0.00073	This work (I)
55708.51460 ± 0.00022	99.0	0.00061	This work (r)
55482.64913 ± 0.00081	18.0	0.00151	Shadic (TRESKA)
55716.87995 ± 0.00086	102.0	0.00054	Garlitz (TRESKA)
55736.39824 ± 0.00091	109.0	-0.00048	Ayiomamitis (TRESKA)
55744.76350 ± 0.00092	112.0	-0.00064	Garlitz (TRESKA)
55761.50126 ± 0.00290	118.0	0.00628	This work (NR)

stars has a negligible impact on the shape of the observed transits. A second-order polynomial was required for the CAHA light curves, but a first-order one was enough for the Cassini data. The resulting photometry is given in Table 2, and reaches a scatter as low as 0.75 mmag for the first Cassini transit. We also obtained the z -band and R -band data presented in Bakos et al. (2007) for inclusion in our analysis. These datasets cover two and four transits, respectively.

3 ANALYSIS

We have measured the physical properties of the HAT-P-5 system using the methods described by Southworth (2008, 2009, 2010, 2011), thus retaining consistency with the *Homogeneous Studies* project results. A detailed description of our approach is given by those works, so we only summarise it briefly below.

² Information on the 1.52 m Cassini Telescope and BFOSC can be found at <http://www.bo.astro.it/loiano/>

³ <http://www.cyanogen.com/>

⁴ The acronym IDL stands for Interactive Data Language and is a trademark of ITT Visual Information Solutions. For further details see <http://www.itervis.com/ProductServices/IDL.aspx>.

⁵ <http://idlastro.gsfc.nasa.gov/>

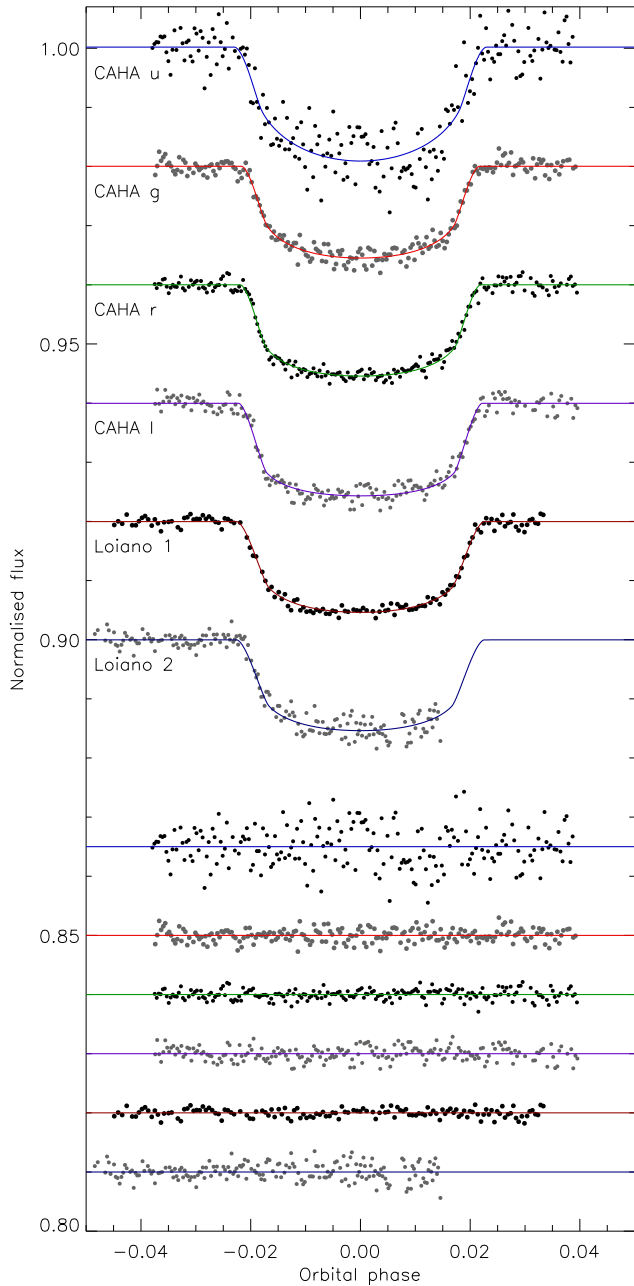


Figure 2. Phased light curves of HAT-P-5 compared to the best JKTEBOP fits using the quadratic limb darkening law. The sources of the light curves are labelled on the plot. The residuals of the fits are plotted at the base of the figure, offset from zero.

3.1 Period determination

As a first step in our analysis we fitted all of the light curves individually using JKTEBOP (see below). The absolute values of the observational errors from our pipeline (which stem ultimately from the APER subroutine) are optimistic, so were rescaled for each dataset to give a reduced χ^2 of $\chi^2_\nu = 1$. The times of mid-transit were then measured, and their uncertainties estimated from Monte Carlo simulations. The second Loiano transit was discounted from this as the data cover only part of the transit event (see Gibson et al. 2009).

To our times of minimum we added 14 timings obtained

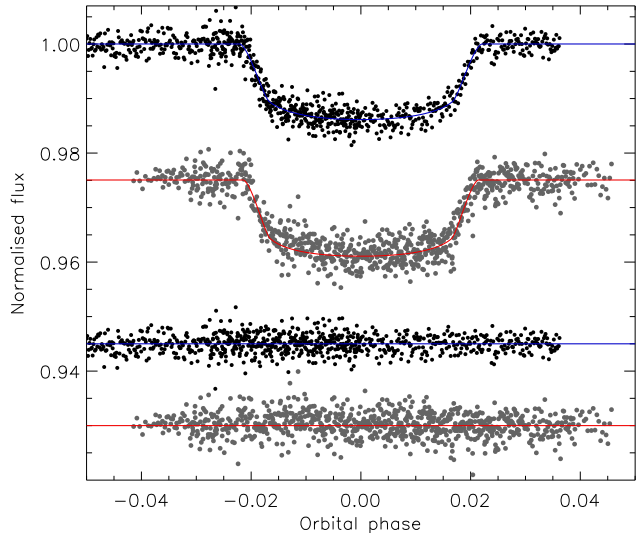


Figure 3. As for Fig. 2 but for the z and R light curves of HAT-P-5 presented by Bakos et al. (2007).

by amateur astronomers and made available on the AXA⁶ and TRESCA⁷ websites. We included only timings based on data of low scatter and covering a full transit. All timings whose timescale is not stated were assumed to be on the UTC system and converted to TDB.

The resulting measurements of transit midpoints were fitted with a straight line to obtain an orbital ephemeris. Cycle zero is specified to be the midpoint of the transit observed at CAHA. We found:

$$T_0 = \text{BJD(TDB)} 2\,455\,432.45510(10) + 2.78847360(52) \times E$$

where E is the number of orbital cycles after the reference epoch and quantities in brackets denote the uncertainty in the final digit of the preceding number. The quality of the fit is $\chi^2_\nu = 1.46$, which implies that a linear ephemeris is not a perfect fit to the transit timings. There is no systematic deviation from the predicted transit times, so we do not regard this as sufficient evidence for transit timing variations. The χ^2_ν is instead interpreted as an indication that the errorbars on the timings are too small, which we have compensated for by increasing the uncertainties in the ephemeris above.

3.2 Light curve modelling

The light curves were modelled using the JKTEBOP⁸ code as described in Southworth (2008). The main information to be gleaned was the fractional radii of the star and planet, $r_A = \frac{R_A}{a}$ and $r_b = \frac{R_b}{a}$, where a is the orbital semimajor axis and R_A and R_b are the true radii of the two objects. The fitted parameters were the sum and ratio of the fractional radii, $r_A + r_b$ and $k = \frac{r_b}{r_A}$, and the orbital inclination, i . A mass ratio of 0.001 was adopted to govern the shapes of the biaxial ellipsoids representing the two component objects. Limb darkening (LD) was imposed using each of five laws and with three choices of whether the LD coefficients were fixed or

⁶ Amateur Exoplanet Archive, <http://brucegary.net/AXA/x.htm>

⁷ The TRansiting ExoplanetS and CANDidates (TRESCA) website can be found at, <http://var2.astro.cz/EN/tresca/index.php>

⁸ JKTEBOP is written in FORTRAN77 and the source code is available at <http://www.astro.keele.ac.uk/~jkt/>

Table 4. Parameters of the JKTEBOP fits to the light curves of HAT-P-5. The final parameters are the weighted means of the results for the six datasets. Results from the literature are included at the base of the table for comparison.

Source	$r_A + r_b$	k	i ($^\circ$)	r_A	r_b
CAHA g -band	0.1407 ± 0.0080	0.1130 ± 0.0025	87.8 ± 1.7	0.1264 ± 0.0069	0.0143 ± 0.0011
CAHA r -band	0.1442 ± 0.0077	0.1165 ± 0.0022	87.7 ± 1.8	0.1292 ± 0.0066	0.0150 ± 0.0010
CAHA I -band	0.1404 ± 0.0059	0.1134 ± 0.0017	88.2 ± 1.5	0.1262 ± 0.0051	0.0143 ± 0.0008
Loiano r -band	0.1562 ± 0.0084	0.1159 ± 0.0026	86.1 ± 1.1	0.1400 ± 0.0073	0.0162 ± 0.0011
Bakos z -band	0.1464 ± 0.0077	0.1094 ± 0.0020	87.2 ± 1.4	0.1320 ± 0.0067	0.0144 ± 0.0010
Bakos R -band	0.1413 ± 0.0095	0.1111 ± 0.0025	87.4 ± 1.9	0.1272 ± 0.0084	0.0141 ± 0.0012
Final results			87.18 ± 0.61	0.1296 ± 0.0027	0.01467 ± 0.00041
Bakos et al. (2007)	0.1477	0.1106 ± 0.0006	86.75 ± 0.44	0.133 ± 0.003	0.01471
Torres et al. (2008)	0.1478	0.1106 ± 0.0006	86.75 ± 0.44	0.1333 ± 0.0033	0.01472

fitted. Uncertainties were calculated using both Monte Carlo simulations (Southworth et al. 2004) and a residual-permutation algorithm (as implemented by Southworth 2008). The larger of the two values was retained for each output quantity. The orbital eccentricity was fixed to zero (Bakos et al. 2007) and contaminating light was taken to be negligible (Daemgen et al. 2009).

The CAHA g , r and I data were solved individually, and the u -band light curve was ignored at this point due to its much greater scatter. The Loiano transits were solved simultaneously but with the orbital period fixed at the value determined in Section 3.1. We also considered the z -band and R -band follow-up data presented in Bakos et al. (2007). In all six cases we found that the best solutions were obtained when fitting for the linear LD coefficient and fixing the nonlinear coefficient at a theoretically-predicted value (but perturbing it by ± 0.1 on a flat distribution during the Monte Carlo and residual-permutation simulations).

An overall set of photometric parameters was calculated for each dataset and is given in Table 4. Tables of individual fits for each light curve are given in the Supplementary Information which accompanies this work. The corresponding best fits are shown in Fig. 2 for the data presented in this work and in Fig. 3 for the data from Bakos et al. (2007). The final photometric parameters are the weighted mean of the values for each dataset. At first glance the Loiano results are outliers, but this impression is not backed up by statistics: the χ_ν^2 value of the agreement of the individual parameters with respect to the weighted mean is 1.5 for k but smaller than 0.6 for the other photometric parameters. Table 4 also shows a comparison with the results from Bakos et al. (2007) and Torres et al. (2008). These authors agree well with our final parameter values, but find errorbars which are notably smaller than ours for those datasets in common.

3.3 Variation of planetary radius with wavelength

Once the final photometric parameters had been established, each light curve was fitted with i and r_A fixed in order to investigate the possibility of a variation of r_b with wavelength. The resulting r_b values should have reliable relative uncertainties from which the common sources of error have been removed. We inflated the errorbars to account for systematic noise following the ‘ β ’ approach and with groups of up to ten consecutive datapoints (e.g. Winn et al. 2007). One issue to bear in mind when fixing i and r_A is that any variations in these parameters, or effects arising from systematic noise, will be concentrated in the remaining free parameters, including r_b .

Whilst r_b *might* vary detectably with wavelength, the LD characteristics of the parent star certainly do. In order to make any errors in the theoretical representation of LD by stellar model atmospheres clear, we calculated r_b values with the linear LD coefficient included as a fitted parameter as well as solutions in which both coefficient were fixed to theoretical values. An excellent discussion of the treatment of LD in transit light curves is given by Howarth (2011).

Fig. 4 shows the variation of r_b with wavelength with the linear LD coefficient fitted (top panel) and fixed (middle panel). The corresponding results are given in Table 5. Clear variations with wavelength are seen, and are robust against the treatment of LD. In all cases fixing LD coefficients leads to r_b values which are smaller, an effect which is most pronounced for the u -band data. Changing the LD coefficients to their physical limits (i.e. the total LD at the limb of the star is zero or unity) cannot shift the u -band r_b into alignment with the other results.

The referee raised concerns that correlated noise in the photometry could be influencing the observed variations in r_b , and that by fixing i and r_A to common values any systematic errors would be concentrated in r_b . We have therefore shown in Fig. 4 (bottom panel) the values of r_b obtained when i and r_A are not constrained to be the same for each light curve. The differences between the three panels in Fig. 4 therefore highlight the effect of adopting a common set of system parameters.

So is the variation of r_b with wavelength real? The two r -band datasets are in good agreement, which is encouraging. The u -band result is very discrepant with those from the other bands, but the reality of this phenomenon is arguable. Of all optical wavelengths, photometry blueward of the Balmer jump suffers the most from the strength and variability of Earth-atmospheric extinction, although the altitude of CAHA (2168 m above sea level) will mitigate that to some extent. u - and U -band photometry is also often handicapped by a lack of comparison stars, which is true in the current case (only one good comparison star compared to at least two for all other bands). Our CAHA observations were also taken at full moon (illuminated fraction 0.994) so the sky background was comparatively high in u and g . Fig. 2 shows that our u -band data have some correlated noise visible in the residuals.

A second suggestion of correlated noise affecting the r_b values is that those for the z - and R -band data are significantly below the values found from our new data. Whilst this could be interpreted as indicative of temporal variation in the properties of the system, it is most likely to herald the presence of systematic errors in the photometry. Further observations are needed to assess the significance of the r_b variations we see. For the remainder of this work we pro-

Table 5. Fractional planetary radius values ($r_b = \frac{R_p}{a}$) found from the available data with the linear limb darkening (LD) coefficient either fitted or fixed, when the other photometric parameters are fixed at their known/final values.

Source	r_b (LD fitted)	r_b (LD fixed)
CAHA <i>u</i> -band	0.01659 ± 0.00031	0.01581 ± 0.00027
CAHA <i>g</i> -band	0.01483 ± 0.00012	0.01464 ± 0.00011
CAHA <i>r</i> -band	0.01500 ± 0.00009	0.01484 ± 0.00007
CAHA <i>I</i> -band	0.01533 ± 0.00014	0.01515 ± 0.00012
Loiano <i>r</i> -band	0.01495 ± 0.00010	0.01475 ± 0.00009
Bakos <i>z</i> -band	0.01434 ± 0.00006	0.01433 ± 0.00005
Bakos <i>R</i> -band	0.01438 ± 0.00008	0.01430 ± 0.00007

ceed under the assumption that the variations of r_b with wavelength are unconfirmed.

3.3.1 Possible explanations of the radius variation

If the observed variations of radius with wavelength were true, what would they imply? The r_B value from the *u*-band data is substantially larger than those in the other passbands, which is in the opposite direction to the predictions of Fortney et al. (2008). Rayleigh scattering causes a larger radius at bluer wavelengths, which would fit the *u* result but not the more modest trend seen in the *g*, *r* and *I* results. Similarly, the sulphur chemistry advocated by Zahnle et al. (2009) would lead to a larger radius in both *u* and *g* due to opacity of HS.

Next, one can calculate the size of the *u*-band radius difference in units of the atmospheric pressure scale height, H . The r_b at *u* is 7% (for fixed LD coefficients) or 11% (linear LD coefficient fitted) larger than that for the *r* band. This equates to a difference of 6100 km or 9700 km. For HAT-P-5 b $H \approx 500$ km (using data from de Pater & Lissauer 2001). The radius variation is therefore roughly $12H$ or $19H$, which is large but not excessive. Sing et al. (2011, their fig. 14) measured radii for HD 189733 b which approached $6H$ larger at 330 nm than that measured by Pont et al. (2008) in the 1000–1025 nm passband. Rayleigh scattering is therefore a plausible explanation.

Two further possibilities are apparent. Firstly, an unusually large transit depth was found for WASP-12 by Fossati et al. (2010) and interpreted as evidence for an extended exosphere surrounding the planet, with the possible presence of a disc formed from excreted material. The observations have subsequently been analysed in the context of a bow shock arising from the motion of the planet through the stellar wind (Vidotto et al. 2010; Llama et al. 2011). The observable consequences of this situation are that UV transits are deeper and begin earlier than those at redder wavelengths. A bow shock would be much weaker due to the larger orbital separation in the HAT-P-5 system (0.04079 ± 0.00080 AU; see below) compared to WASP-12 (0.02293 ± 0.00078 AU; Hebb et al. 2009; Chan et al. 2011). Whilst our observations satisfy the criterion of a deeper transit at bluer wavelengths, they do not indicate that the *u* transit occurs earlier than the *g*, *r* and *I* ones (see Table 3).

The second possibility is that the stellar surface exhibited starspots during our observations, which are not directly detectable because they were not occulted by the planet. This would act to increase the depth of the transit. If the temperature of the spot(s) is close enough to the T_{eff} of the star that they contribute significant flux at redder wavelengths, this would induce a wavelength dependence such that transits in the blue are deeper than those in the red.

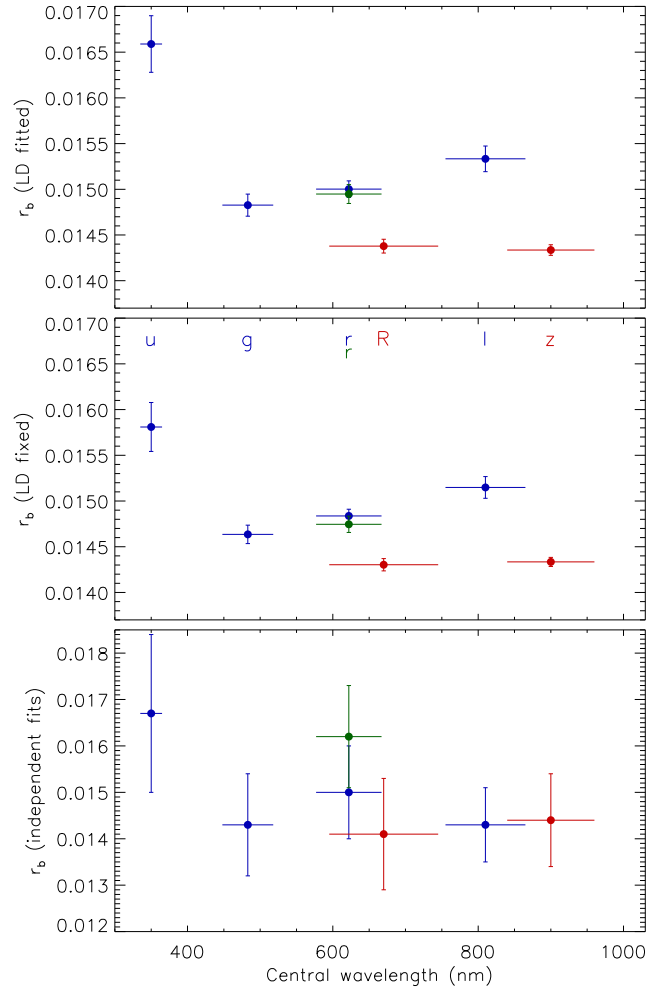


Figure 4. Variation of the fractional planetary radius ($r_b = \frac{R_p}{a}$) with wavelength. Results from the CAHA data are shown in blue, from Loiano in green, and from the Bakos et al. (2007) data in red. The vertical lines represent the relative errors in the measurements and the horizontal lines show the full widths at half maximum transmission of the passbands used. The top panel gives the results for limb darkening fitted, the middle panel for LD fixed at theoretically predicted values, and the lower panel shows the results when the system parameters are not forced to be the same for different light curves. The filter designations are labelled at the top of the lower panel.

Such a phenomenon would explain both a deeper *u*-band transit and a greater transit depth overall compared to those in Bakos et al. (2007). However, it does not agree well with the observed trend in the *g*, *r* and *I* bands. The level of starspot activity would also have to be similar at both of our *r*-band epochs, which are separated by nine months, in order to explain their mutual agreement.

The spot activity of HAT-P-5A can be investigated using time-series photometry extending over a significant time interval. The SuperWASP archive (Pollacco et al. 2006; Butters et al. 2010) lists 48 392 observations of HAT-P-5 over the years 2004 to 2010. We searched these data for periodicities indicative of spot-induced rotational modulation, using the method of Maxted et al. (2011). The periodograms of the data show only peaks near 1 d and 28 d, which we attribute to the diurnal and lunar cycles. We set a 95%-confidence upper limit of 0.5 mmag on rotational modulations, which confirms that HAT-P-5 is a quiet star.

Table 6. Derived physical properties of the HAT-P-5 system. For each set of physical properties the following quantities are the same: $g_b = 16.7 \pm 1.9 \text{ m s}^{-2}$, $\rho_A = 0.791 \pm 0.050 \rho_\odot$ and $T'_{\text{eq}} = 1517 \pm 29 \text{ K}$.

	This work (dEB constraint)	This work (Claret models)	This work (Y^2 models)	This work (Teramo models)	This work (VRSS models)	This work (DSEP models)
K_b (km s^{-1})	162.2 ± 4.9	159.8 ± 1.9	159.1 ± 2.3	158.6 ± 2.9	158.0 ± 2.4	158.5 ± 3.0
M_A (M_\odot)	1.240 ± 0.113	1.185 ± 0.042	1.170 ± 0.051	1.159 ± 0.063	1.147 ± 0.052	1.156 ± 0.065
R_A (R_\odot)	1.161 ± 0.044	1.144 ± 0.029	1.139 ± 0.029	1.135 ± 0.031	1.132 ± 0.029	1.135 ± 0.032
$\log g_A$ (cgs)	4.402 ± 0.021	4.395 ± 0.019	4.393 ± 0.019	4.392 ± 0.020	4.390 ± 0.020	4.392 ± 0.020
M_b (M_{Jup})	1.10 ± 0.13	1.07 ± 0.11	1.06 ± 0.11	1.06 ± 0.11	1.05 ± 0.11	1.05 ± 0.11
R_b (R_{Jup})	1.279 ± 0.053	1.260 ± 0.039	1.254 ± 0.040	1.250 ± 0.042	1.246 ± 0.040	1.250 ± 0.042
ρ_b (ρ_{Jup})	0.494 ± 0.067	0.501 ± 0.066	0.503 ± 0.067	0.505 ± 0.067	0.507 ± 0.067	0.505 ± 0.067
Θ	0.0580 ± 0.0064	0.0589 ± 0.0063	0.0591 ± 0.0063	0.0593 ± 0.0063	0.0595 ± 0.0063	0.0594 ± 0.0064
a (AU)	0.04166 ± 0.00126	0.04104 ± 0.00049	0.04086 ± 0.00059	0.04073 ± 0.00074	0.04059 ± 0.00061	0.04070 ± 0.00076

Table 7. Final physical properties of the HAT-P-5 system, compared with results from the literature. Where two errorbars are given, the first refers to the statistical uncertainties and the second to the systematic errors.

	This work (final)	Bakos et al. (2007)	Torres et al. (2008)
M_A (M_\odot)	$1.163 \pm 0.065 \pm 0.022$	1.160 ± 0.062	$1.157^{+0.043}_{-0.081}$
R_A (R_\odot)	$1.137 \pm 0.032 \pm 0.007$	1.167 ± 0.049	$1.165^{+0.046}_{-0.052}$
$\log g_A$ (cgs)	$4.392 \pm 0.020 \pm 0.003$	4.368 ± 0.028	$4.368^{+0.025}_{-0.031}$
ρ_A (ρ_\odot)	0.791 ± 0.050		$0.729^{+0.058}_{-0.054}$
M_b (M_{Jup})	$1.06 \pm 0.11 \pm 0.01$	1.06 ± 0.11	$1.06^{+0.11}_{-0.11}$
R_b (R_{Jup})	$1.252 \pm 0.042 \pm 0.008$	1.257 ± 0.053	$1.254^{+0.051}_{-0.056}$
g_b (m s^{-2})	16.7 ± 1.9	16.5 ± 1.9	$16.6^{+1.9}_{-1.8}$
ρ_b (ρ_{Jup})	$0.504 \pm 0.067 \pm 0.003$	0.50 ± 0.08	$0.50^{+0.09}_{-0.08}$
T'_{eq} (K)	1517 ± 29		1539^{+33}_{-32}
Θ	$0.0592 \pm 0.0064 \pm 0.0004$		$0.0591^{+0.0064}_{-0.0062}$
a (AU)	$0.04079 \pm 0.00076 \pm 0.00026$	0.04075 ± 0.00076	$0.04071^{+0.00049}_{-0.00097}$
Age (Gyr)	$1.7^{+3.5+0.4}_{-1.4-0.6}$	2.6 ± 1.8	$2.6^{+2.1}_{-1.4}$

In conclusion, we observe a different transit depth in u compared to g , r and I . We also find lower transit depths for the R and z observations obtained by Bakos et al. (2007). We have attempted to interpret these effects in the context of a variation of opacity with wavelength in the planetary atmosphere, the presence of a bow shock, or spot activity on the host star. None of these possibilities provide a completely satisfactory description of the data, but Rayleigh scattering remains plausible. Our preferred explanation is that the differences in transit depth are due to systematic effects in the available photometry.

3.4 Physical properties of the HAT-P-5 system

We determined the physical properties of the HAT-P-5 system using the approach described in Southworth (2009). Starting with the measured photometric parameters and known orbital velocity amplitude of the star ($K_A = 138 \pm 14 \text{ m s}^{-1}$; Bakos et al. 2007), we guessed a velocity amplitude for the planet (K_b) and used standard formulae (e.g. Hilditch 2001) to obtain an estimate of the properties of the system. These comprise the mass, radius, surface gravity and mean density for the star (M_A , R_A , $\log g_A$ and ρ_A) and planet (M_b , R_b , g_b and ρ_b), and the orbital semimajor axis (a). We then interpolated within the predictions of theoretical stellar models to find the effective temperature (T_{eff}) and R_A corresponding to the estimated M_A and measured metallicity ($[F_{\text{Fe}}/H] = 0.24 \pm 0.15$; Bakos et al. 2007). The value of K_b was then iteratively refined

to maximise the agreement between the estimated and observed T_{eff} ($5960 \pm 100 \text{ K}$; Bakos et al. 2007), and the estimated $\frac{R_A}{a}$ and known r_A . This process was performed for a grid of ages starting from the zero-age main sequence and stepping in 0.01 Gyr chunks until the star had evolved to a $\log g$ less than 3.5. The final result was a set of physical properties and a system age which gave the best agreement with the known T_{eff} and r_A .

The random errors in this process were propagated via a perturbation analysis (Southworth et al. 2005). Our use of theoretical models inevitably incurs a systematic error due to the dependence on stellar theory. We assessed these systematic errors from the intercomparison of sets of physical properties calculated using each of five independent sets of stellar models (Southworth 2011). Our final result for each physical property corresponds to the unweighted mean of the five different values, whilst its statistical error is the largest of the five possibilities and its systematic error is the standard deviation of the values from the five models. Note that three quantities are independent of stellar theory so are not troubled by systematic errors: g_b (Southworth et al. 2007), ρ_A (Seager & Mallén-Ornelas 2003) and T'_{eq} (Southworth 2009).

It is possible to avoid using stellar models by recourse to calibrations based on empirical measurements of stars in eclipsing binary systems (Southworth 2009). We adopted the approach outlined by Enoch et al. (2010) but with the improved calibration coefficients calculated by Southworth (2011). The set of physical properties resulting from this method are shown in Table 6, along

with the five sets arriving from the use of stellar models. Our final properties are given in Table 7. The results obtained by Bakos et al. (2007) and Torres et al. (2008) are in very close agreement with our own, despite being based on much sparser photometric data.

4 SUMMARY

We present photometry of four transit events in the HAT-P-5 extra-solar planetary system, obtained using telescope-defocussing techniques and reaching scatters as low as 0.75 mmag per point. One of these transits was observed in four passbands simultaneously, using the BUSCA imager on the CAHA 2.2 m telescope. We used these data to improve the measured orbital ephemerides and physical properties of the system. HAT-P-5 is well-characterised, although it would benefit from further observations to refine the spectroscopic orbit and atmospheric properties of the host star. The planet is slightly too large to match the predicted radii of coreless gaseous planets (Fortney et al. 2007; Baraffe et al. 2008), confirming its status as an inflated hot Jupiter. HAT-P-5 becomes the sixtieth TEP system to be studied as part of the *Homogeneous Studies* project (Southworth 2008) and its physical properties have been placed in the Transiting Extrasolar Planets Catalogue⁹

Both components of HAT-P-5 have similar temperatures to those in the prototype transiting system HD 209458, so the planets are expected to have similar atmospheric characteristics. We used our multi-band photometry to search for variations of the measured planetary radius with wavelength, which could indicate the presence of Rayleigh scattering or the opacity of specific molecules. We find that the radius in the *u* band is significantly larger than at the other optical wavelengths, by either 12 or 19 pressure scale heights depending on the treatment of limb darkening when fitting the light curves. We also find that the planet radius measured in earlier *R* and *z*-band data is smaller than that from our data. These phenomena are most likely due to the presence of systematic errors in the photometric data. Alternative possibilities include Rayleigh scattering and temporal changes in the system properties, but explanations involving starspots or a bow shock do not match existing observations.

ACKNOWLEDGMENTS

Based on observations collected at the Centro Astronómico Hispano Alemán (CAHA) at Calar Alto, Spain, operated jointly by the Max-Planck Institut für Astronomie and the Instituto de Astrofísica de Andalucía (CSIC), and on observations obtained with the 1.5 m Cassini telescope at Loiano Observatory, Italy. The reduced light curves presented in this work will be made available at the CDS (<http://cdsweb.u-strasbg.fr/>) and at <http://www.astro.keele.ac.uk/~jkt/>. JS acknowledges financial support from STFC in the form of an Advanced Fellowship. We thank Roberto Gualandi for his technical assistance at the Cassini telescope, Simona Ciceri for taking part to these observations, and Nikolay Nikolov for suggesting the bow-shock explanation. The following internet-based resources were used in research for this paper: the ESO Digitized Sky Survey; the NASA Astrophysics Data System; the SIMBAD database operated at CDS, Strasbourg, France; and the arXiv scientific paper preprint service operated by Cornell University.

REFERENCES

- Bakos, G. Á., et al., 2007, *ApJ*, 671, L173
 Baraffe, I., Chabrier, G., Barman, T., 2008, *A&A*, 482, 315
 Barman, T., 2007, *ApJ*, 661, L191
 Batygin, K., Bodenheimer, P., Laughlin, G., 2009, *ApJ*, 704, L49
 Brown, T. M., Charbonneau, D., Gilliland, R. L., Noyes, R. W., Burrows, A., 2001, *ApJ*, 552, 699
 Burrows, A., Hubeny, I., Budaj, J., Hubbard, W. B., 2007, *ApJ*, 661, 502
 Burrows, A., Rauscher, E., Spiegel, D. S., Menou, K., 2010, *ApJ*, 719, 341
 Butters, O. W., et al., 2010, *A&A*, 520, L10
 Chan, T., Ingemyr, M., Winn, J. N., Holman, M. J., Sanchis-Ojeda, R., Esquerdo, G., Everett, M., 2011, *AJ*, 141, 179
 Charbonneau, D., Brown, T. M., Noyes, R. W., Gilliland, R. L., 2002, *ApJ*, 568, 377
 Daemgen, S., Hormuth, F., Brandner, W., Bergfors, C., Janson, M., Hippler, S., Henning, T., 2009, *A&A*, 498, 567
 de Pater, I., Lissauer, J. J., 2001, *Planetary Sciences*, by Imke de Pater and Jack J. Lissauer, Cambridge University Press, Cambridge, UK
 Eastman, J., Siverd, R., Gaudi, B. S., 2010, *PASP*, 122, 935
 Enoch, B., Collier Cameron, A., Parley, N. R., Hebb, L., 2010, *A&A*, 516, A33
 Fortney, J. J., Marley, M. S., Barnes, J. W., 2007, *ApJ*, 659, 1661
 Fortney, J. J., Lodders, K., Marley, M. S., Freedman, R. S., 2008, *ApJ*, 678, 1419
 Fossati, L., et al., 2010, *ApJ*, 714, L222
 Gibson, N. P., et al., 2009, *ApJ*, 700, 1078
 Hebb, L., et al., 2009, *ApJ*, 693, 1920
 Hilditch, R. W., 2001, *An Introduction to Close Binary Stars*, Cambridge University Press, Cambridge, UK
 Howarth, I. D., 2011, *MNRAS*, in press, [arXiv:1106.4659](https://arxiv.org/abs/1106.4659)
 Knutson, H. A., Charbonneau, D., Noyes, R. W., Brown, T. M., Gilliland, R. L., 2007, *ApJ*, 655, 564
 Krivov, A. V., Reidemeister, M., Fiedler, S., Löhne, T., Neuhäuser, R., 2011, *MNRAS*, 418, L15
 Llama, J., Wood, K., Jardine, M., Vidotto, A. A., Helling, C., Fossati, L., Haswell, C. A., 2011, *MNRAS*, 416, L41
 Maxted, P. F. L., et al., 2011, *PASP*, 123, 547
 Pollacco, D. L., et al., 2006, *PASP*, 118, 1407
 Pont, F., Knutson, H., Gilliland, R. L., Moutou, C., Charbonneau, D., 2008, *MNRAS*, 385, 109
 Seager, S., Mallén-Ornelas, G., 2003, *ApJ*, 585, 1038
 Sing, D. K., Vidal-Madjar, A., Désert, J.-M., Lecavelier des Etangs, A., Ballester, G., 2008, *ApJ*, 686, 658
 Sing, D. K., et al., 2011, *MNRAS*, 416, 1443
 Southworth, J., 2008, *MNRAS*, 386, 1644
 Southworth, J., 2009, *MNRAS*, 394, 272
 Southworth, J., 2010, *MNRAS*, 408, 1689
 Southworth, J., 2011, *MNRAS*, 417, 2166
 Southworth, J., Maxted, P. F. L., Smalley, B., 2004, *MNRAS*, 351, 1277
 Southworth, J., Maxted, P. F. L., Smalley, B., 2005, *A&A*, 429, 645
 Southworth, J., Wheatley, P. J., Sams, G., 2007, *MNRAS*, 379, L11
 Southworth, J., Bruni, I., Mancini, L., Gregorio, J., 2011, *MNRAS*, in press, [arXiv:1111.5432](https://arxiv.org/abs/1111.5432)
 Southworth, J., et al., 2009a, *MNRAS*, 396, 1023
 Southworth, J., et al., 2009b, *MNRAS*, 399, 287

⁹ TEPcat: <http://www.astro.keele.ac.uk/~jkt/tepcat/>

- Southworth, J., et al., 2010, MNRAS, 408, 1680
Stetson, P. B., 1987, PASP, 99, 191
Torres, G., Winn, J. N., Holman, M. J., 2008, ApJ, 677, 1324
Vidotto, A. A., Jardine, M., Helling, C., 2010, ApJ, 722, L168
Winn, J. N., et al., 2007, AJ, 134, 1707
Zahnle, K., Marley, M. S., Freedman, R. S., Lodders, K., Fortney,
J. J., 2009, ApJ, 701, L20